Since January 2020 Elsevier has created a COVID-19 resource centre with free information in English and Mandarin on the novel coronavirus COVID-19. The COVID-19 resource centre is hosted on Elsevier Connect, the company's public news and information website.

Journal of Molecular Structure 1244 (2021) 130967

Contents lists available at ScienceDirect

Journal of Molecular Structure

journal homepage: www.elsevier.com/locate/molstr

(*2E*)-2-(4-ethoxybenzylidene)-3,4-dihydro-*2H*-naphthalen-1-one single crystal: Synthesis, growth, crystal structure, spectral characterization, biological evaluation and binding interactions with SARS-CoV-2 main protease

N. Afsar[a,b,*], D. Reuben Jonathan[c], B.K. Revathi[d], Dhurairaj Satheesh[b], S. Manivannan[a]

[a] Dr. Ambedkar Government Arts College (Autonomous), Chennai 600 039, Tamilnadu, India
[b] Loganatha Narayanasamy Government College (Autonomous), Ponneri 601 204, Tamilnadu, India
[c] Department of Chemistry, Madras Christian College (Autonomous), Chennai 600 059, Tamilnadu, India
[d] Department of Physics, Madras Christian College (Autonomous), Chennai 600 059, Tamilnadu, India

ARTICLE INFO

Article history:
Received 11 March 2021
Revised 20 June 2021
Accepted 22 June 2021
Available online 24 June 2021

Keywords:
Claisen-Schmidt condensation
Chalcone
Crystal growth
Crystal structure
Biological activity
SARS-CoV-2

ABSTRACT

A new α-Tetralone based chalcone compound, (2E)-2-(4-ethoxybenzylidene)-3,4-dihydro-2H-naphthalen-1-one (**EBDN**) has been synthesized by Claisen–Schmidt condensation reaction of α-Tetralone (**1**) with 4-Ethoxybenzaldehyde (**2**) in basic medium. Then it was allowed to grow through slow evaporation solution growth technique. The molecular structure of grown **EBDN** has been systematically characterized by SCXRD, FT-IR, ^{1}H NMR and ^{13}C NMR spectroscopic studies. The micro-hardness, thermal (TGA & DTA) and photoluminence studies of the synthesized **EBDN** were also examined. The **EBDN** was screened for its anti-inflammatory, antidiabetic and anti-oxidant activity. It has shown admirable anti-inflammatory and antidiabetic activity. Protein-Ligand interactions of **EBDN** with SARS-CoV-2 main protease (PDB code: **6yb7**) also performed.

1. Introduction

Chalcones ((E)-1,3-diphenylprop-2-ene-1-ones, Fig. 1) are one of the most overbearing classes and a modest chemical scaffolding of numerous naturally occurring compounds across the plant kingdom (vegetables, spices, fruits, teas and etc.,) [1–6]. Chalcones belong to the family of flavonoids and they are also known as chalconoids. Which exhibits geometrical isomers cis and trans, and the thermodynamically more stable one is the trans isomer (Fig. 1).

Chalcones are organic compounds possessing acceptor and donor groups, which enhance their importance in various fields. The chalcone compounds have attained significance because of their excellent NLO properties [7]. The NLO response was found to increase as the donor strength of the molecules increased.

The chalcone family has drawn a lot of attention not only from synthetic and biosynthetic perspectives, but also from pharmacological applications because they have revealed a lot of biological actions that include the treatment of medical disorders like microbial and viral infections [8–11], cancer [12–15], cardiovascular diseases and their risk factors [16–19], anti-inflammatory [20] and antioxidant activities [21,22]. The maximum reactive moiety is due to the, [23] α,β-unsaturated carbonyl bridge, which is related to chalcone biological actions [24]. Some chalcone-moiety containing compounds have additionally been permitted for clinical use. For example, metochalcone ((E)-1-(2,4-dimethoxyphenyl)-3-(4-methoxyphenyl) prop-2-en-1-one) was approved as a choleretic while sofalcone was approved as an antiulcer and mucoprotective drug (Fig. 1) [25,26].

1-Tetralones are an essential elegance of compounds, and their numerous derivatives have proven important biological applications, including antimicrobial activity [27], anti-tumor activity [28], and neurological disorders. [29,30,43] Several (E)-2-(4′-substitutedbenzylidene)-1-tetralones (Fig. 2) have been synthesized, characterized by using spectroscopic tools and also performed their biological applications [31–38].

Since it's unveiling at the end of December 2019, SARS-CoV-2 has remained to spread chop-chop throughout the world. Despite the fact that the number of deaths caused by COVID-19 is rapidly increasing, an effective drug treatment other than vaccines has yet to be developed.The existing literature comprises many investi-

* Corresponding author.
E-mail address: afsar.noorullah@gmail.com (N. Afsar).

https://doi.org/10.1016/j.molstruc.2021.130967
0022-2860/

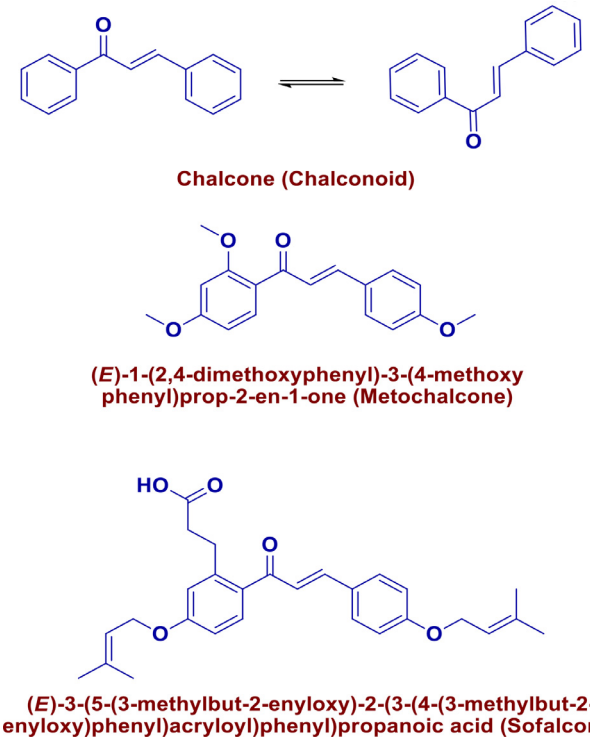

Fig. 1. Structure representation of chalcone and two clinically approved chalcone moiety containing drugs.

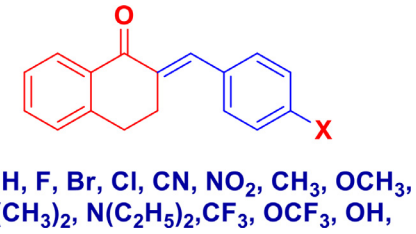

Fig. 2. Structure representation of 1-Tetralone based chalcones.

gations on SARS-CoV-2 main protease and its potential inhibitors [39–45].

In this present investigation, a new α-Tetralone based chalcone compound, (2E)-2-(4-ethoxybenzylidene)-3,4-dihydro-2H-naphthalen-1-one **(EBDN**) has been synthesized and grown through a slow evaporation solution growth technique. The molecular structure of grown **EBDN** has been characterized by SCXRD, FT-IR, ^{1}H NMR and ^{13}C NMR spectroscopic studies. The microhardness, thermal (TGA & DTA) and photoluminence studies were also examined. The **EBDN** was screened for its anti-inflammatory, antidiabetic and anti-oxidant activity. Protein-Ligand interactions of **EBDN** with SARS-CoV-2 main protease also performed.

2. Experimental methods

2.1. Materials

α-tetralone (97%, Sigma Aldrich), *p*-Ethoxy benzaldehyde (99%, Sigma Aldrich), Absolute alcohol and sodium hydroxide (Spectrochem) were purchased from commercially available and were used.

2.2. Methods

2.2.1. Synthesis of (2E)-2-(4-ethoxybenzylidene)-3,4-dihydro-2H-naphthalen-1-one

In a 250 mL round-bottomed flask, α-tetralone (0.05 mol, 7.3 mL) and *p*-ethoxy benzaldehyde (0.05 mol, 7.0 mL) were taken to which 100 mL of absolute alcohol was added and stirred well for complete dissolution. After a span of 10 min, about 10 mL of 10% sodium hydroxide solution was added and the solution was stirred for about 1 hour at room temperature. After 12 h, ice cold water was added to precipitate the obtained light yellow color product which was filtered, washed with double distilled water and dried (Scheme 1: Yield: 85%, 11.8297 g).

EBDN: Light yellow single crystal. m.p.: 141–142 °C. **^{1}H NMR** (δ in ppm, $CDCl_3$, 400 MHz): 8.13, 8.10 (d, 1H, J = 12 Hz), 7.84 (s, 1H), 7.49, 7.47 (d, 1H, J = 8 Hz), 7.45–7.40 (dd, 2H, J = 20 Hz), 7.37–7.33 (m, 1H, J = 16 Hz), 7.25, 7.23 (d, 1H, J = 8 Hz), 6.94, 6.92 (d, 2H, J = 8 Hz), 4.10–4.05 (q, 2H, J = 20 Hz), 3.15–3.13 (t, 2H, J = 8 Hz), 2.96–2.93 (t, 2H, J = 12 Hz), 1.45–1.41 (t, 3H, J = 16 Hz). **^{13}C NMR** (δ in ppm, $CDCl_3$, 400 MHz): 188.07 (C=O), 159.59 (**C_{15}**), 143.13 (**C_5**), 136.97 (**C_{11}**), 133.97 (**C_6** & **C_9**), 133.62 (**C_2**), 131.97 (**C_{13}** **& C_{17}**), 128.45 (**C_1**), 128.35 (**C_4**), 128.27 (**C_{12}**), 127.16 (**C_3**), 114.67 (**C_{14}** & **C_{16}**), 63.77 (**C_{18}**), 29.01 (**C_8**), 27.43 (**C_7**), 14.98 (**C_{19}**).

2.2.2. Crystal growth (slow evaporation solution method)

The slow evaporation solution method [38] was adopted to crystallize the formed chalcone. About one gram of the synthesized EBDN was taken in a 100 mL beaker to which 50 mL of acetone was added and then stirred at room temperature for about half-an-hour. Then it was filtered and the filtrate was collected in a 100 mL beaker. It was allowed to undergo slow evaporation at room temperature. When all the solvent was evaporated, the crystals were harvested and dried for crystallographic study (Fig. 3).

2.2.3. Characterization techniques

2.2.3.1. Single crystal X-Ray diffraction studies. X-ray diffraction data for the crystalline EBDN was collected by employing a Bruker APEX DUO CCD diffractometer with a graphite monochromatic Mo-Kα radiation at a detector distance of 5 cm with APEX2 software [46]. The collected data was reduced using the SAINT program and the empirical absorption corrections were performed with the SADABS program. The molecular structure of the (2E)-2-(4-ethoxybenzylidene)-3,4-dihydro-2H-naphthalen-1-one **(EBDN)** crystalline was solved by direct methods and was refined using a full-matrix least-squares method on F2 using the SHELXTL program (Fig. 4) [46].

2.2.3.2. FT-IR spectral analysis. The FT-IR spectrum of the grown crystal **EBDN** was recorded in the wave number region from 400 to 4000 cm^{-1} using a Perkin Elmer FT-IR spectrometer by KBr pellet technique.

2.2.3.3. NMR spectral analysis. ^{1}H NMR and ^{13}C NMR spectrum of the synthesized grown crystal **EBDN** was recorded by using have been Bruker AV 400 NMR spectrometer (400 MHz) in $CDCl_3$.

2.2.4. Biological evaluation

2.2.4.1. Anti-inflammatory analysis (BSA denaturation technique). The grown chalcone compound **EBDN** and standard diclofenac sodium were screened for anti-inflammatory activity in five different concentrations (10, 25, 50, 125 & 250 μg/mL) by using the inhibition of albumin denaturation technique [47] with minor modification. The standard drug and compound were dissolved in a minimum quantity of Dimethyl formamide (DMF) and diluted with phosphate buffer (0.2 M, PH 7.4). The final concentration of DMF

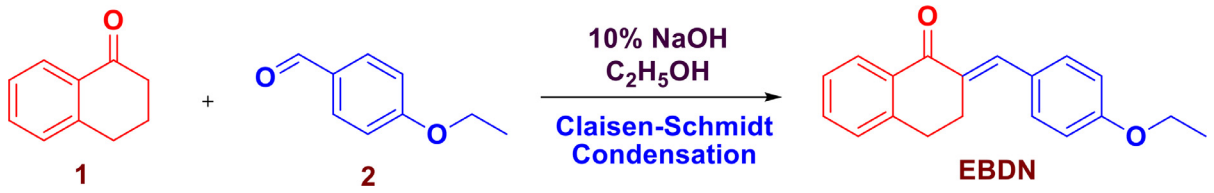

Scheme 1. Synthesis of (*2E*)-2-(4-ethoxybenzylidene)-3,4-dihydro-*2H*-naphthalen-1-one.

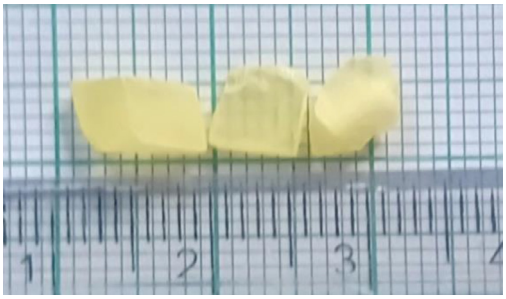

Fig. 3. Photograph of the Grown Crystal of EBDN.

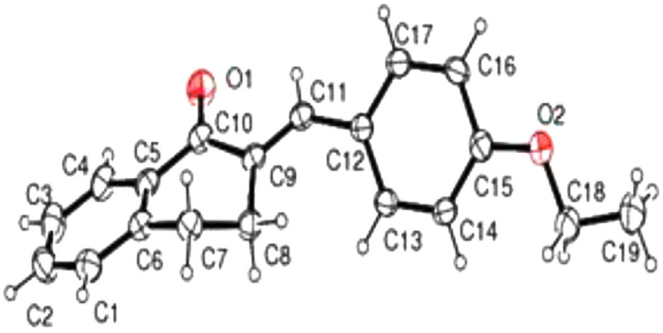

Fig. 4. ORTEP diagram of crystalline EBDN.

in all solutions was less than 2.5%. Test Solution (4 mL) containing different concentrations of the drug was mixed with 1 mL of 1 mM Bovine serum albumin solution in phosphate buffer and incubated at 37 °C in an incubator for 15 min. Denaturation was induced by keeping the reaction mixture at 70 °C in a water bath for 30 min. After cooling, the turbidity was measured at 660 nm. The percentage of inhibition of denaturation was calculated from control where no drug was added. The percentage inhibition of denaturation was calculated by using the following formula.

$$\%\,\text{ofInhibition} = 100 \times [A_c - A_t/A_c]$$

A_t: Absorbance of test
A_c: Absorbance of control

2.2.4.2. Anti-diabetic analysis (α-amylase inhibition technique). The antidiabetic activity of the grown chalcone compound **EBDN** and standard Acarbose in five different concentrations (10, 25, 50, 125 & 250 μg/mL) were performed using α-amylase inhibition method [47]. Briefly, Amylase (0.5 mg/mL) was incubated with and without extract and standard for 10 min at 25 °C. This experiment was performed in 20 mM sodium phosphate buffer (pH 6.9). After pre incubation, the 1% starch solution (1 mL) was added and the reaction mixture was incubated for 30 min at 25 °C. In order to stop the enzymatic reaction, DNSA reagent (1 mL) was added as the color reagent and then incubated in a boiling water bath for15 min. After cooling down to the room temperature, the absorbance measured at 540 nm using a spectrophotometer instrument. The measured absorbance was compared with that of the control experiment. The percentage inhibition was calculated from the given formula.

$$\%\,\text{ofInhibition} = 100 \times [A_c - A_t/A_t]$$

A_t: Absorbance of test
A_c: Absorbance of control

2.2.4.3. Total antioxidant activity (phosphomolybdenum method). Total antioxidant activity of the grown chalcone compound **EBDN** and standard Vitamin C in five different concentrations (10, 25, 50, 125 & 250 μg/mL) were observed using phosphomolybdenum method. About 3 mL of antioxidant reagent (0.6 M H_2SO_4, 28 mM Na_3PO_4 and 4 mM ammonium molybdate) were added to the test samples with various concentrations. The test mixture to accomplish proper diffusion with phosphomolybdenum reagent was incubated at 95 °C for 90 min in a water bath. The total antioxidant activity of extracts and vitamin C standard drug were measured and determined their absorbance at 695 nm using a spectrophotometer. The total antioxidant activities were calculated using the given formula.

$$\text{TOA} = [(A_t - A_c)/A_t] \times 100$$

A_t: Absorbance of test
A_c: Absorbance of control

2.2.5. Protein-ligand interactions

The 3D structure of the SARS-Cov-2 main protease enzyme (**6yb7**.pdb) was downloaded from the protein data bank [48]. The molecular docking poses are visualization using discovery studio. Molecular docking was performed using the Auto-Dock Tool (1.5.6). The 3D structure of EBDN was optimized using Gaussian 09 W [49]. All avoidable water and ligand were removed from the enzyme and polar hydrogen was added to the enzyme. The target was generated as a PDBQT format. PDBQT file of the ligands also generated and performed. The grid box size is fixed as 60 × 60 × 60 points in X, Y, and Z directions. Similarly, the grid space is fixed as 0.375 Å and ten runs were created by using Lamarckian genetic algorithm searches. The default docking parameters were fixed and performed.

3. Results and discussion

3.1. Synthesis and crystal growth of EBDN

The title chalcone compound (2E)-2-(4-ethoxybenzylidene)-3,4-dihydro-2H-naphthalen-1-one (**EBDN**) was successfully synthesized by the simple Claisen-Schmidt condensation reaction of α-Tetralone with 4-ethoxybenzaldehyde in a basic medium (Scheme 1). 85% of EBDN were obtained. Then it was grown through a slow evaporation solution growth technique. The single crystal of grown EBDN was obtained.

3.2. Characterization of EBDN

The molecular structure of the title chalcone compound (*2E*)-2-(4-ethoxybenzylidene)-3,4-dihydro-*2H*-naphthalen-1-one (**EBDN**) was successfully confirmed and characterized by SCXRD, FT-IR and NMR spectral analysis.

Table 1
Crystal data and structure refinement for the EBDN crystal.

CCDC No.	1954163
Identification code	EBDN
Empirical formula	C_{19} H_{18} O_2
Formula weight	278.33
Temperature	296(2) K
Wavelength	0.71073 Å
Crystal system	Monoclinic
Space group	$P2_1$
Unit cell dimensions	a = 6.9532(6) Å α = 90°
	b = 14.8211(14) Å β = 101.969(3)°
	c = 14.5529(13) Å γ = 90°
Volume	1467.1(2) Å^3
Z	4
Density (calculated)	1.260 mg/mm^3
Absorption coefficient	0.080 mm^{-1}
F (000)	592
Crystal size	0.200 × 0.150 × 0.150 mm^3
Theta range for data collection	2.749 to 25.133°
Index ranges	−7<=h<=8, −17<=k<=17, −17<=l<=17
Reflections collected	23,021

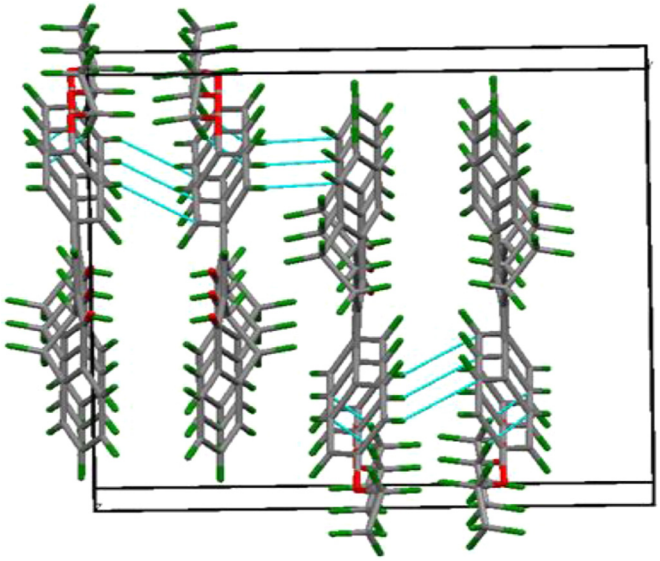

Fig. 5. Crystal packing of Crystalline EBDN.

3.2.1. Single crystal X-ray diffraction study of EBDN

The title chalcone compound, (2E)-2-(4-ethoxybenzylidene)-3,4-dihydro-2H-naphthalen-1-one (EBDN) crystallizes in a monoclinic crystal system with $P2_1/n$ space group with the unit cell parameters shown in Table 1. The crystal packing of the compound viewed along the 'b' axis is presented in Fig. 5.

The molecule exists in an E configuration with respect to the C_9=C_{11} double bond and the dihedral angle existing between the mean plane of the two phenyl rings is 34.4°. The bond lengths and angles are within the normal ranges and comparable with the previously reported structures of chalcone [38]. Table 2 provides experimental values of the bond lengths and bond angles of the synthesised compound molecular structure.

3.2.2. FTIR spectral charatcerization

The FT-IR spectrum and vibrational frequencies of grown EBDN are shown in Fig. 6 and Table 3. For the FT-IR spectrum of EBDN, the aromatic and aliphatic C–H stretching vibrations are observed at 3068 and 2960 cm^{-1} respectively [38,50]. The strong peak was observed at 1675 cm^{-1} which is due to the C=O group of the tetralone moiety [38]. A very strong peak at 1599 cm^{-1} is shown which is attributed to the C=C and C=O groups. The C=C group

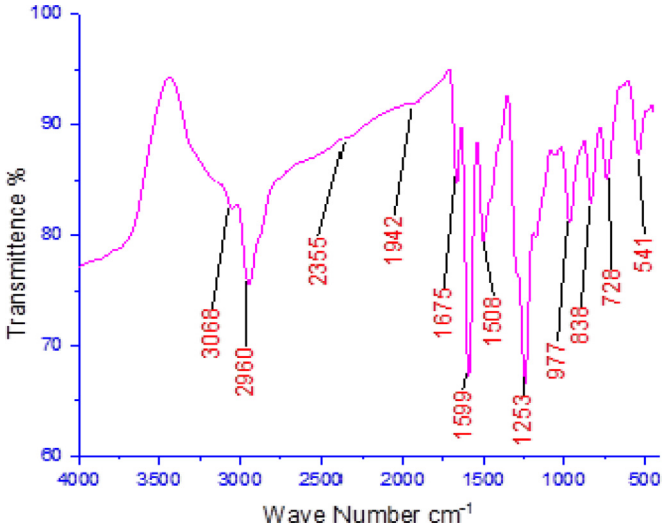

Fig. 6. FT-IR spectrum of grown EBDN.

has also shown a very strong peak at 1508 cm^{-1}. The C–O group is shown a very strong peak at 1253 cm^{-1}. The C–H vibrations were observed at 977, 838, 728 and 541 cm^{-1} [38].

3.2.3. NMR spectral charatcerization

The ^{1}H NMR and ^{13}C NMR spectra of the title compound EBDN was recorded in $CDCl_3$ at 400 MHz and its neat spectrum is shown in Figs. 7 and 8.

3.2.3.1. ^{1}H NMR spectral charatcerization. The ^{1}H NMR spectrum of the title compound, EBDN, is shown.A triplet peaks at 1.41–1.45 ppm and a quartet peaks at 4.10–4.05 ppm are attributed to the methyl and methylene protons of the ethoxy group present in the 4-ethoxybenzylidene moiety respectively [51]. For the 4-ethoxybenzylidene moiety, two aromatic protons (C_{13}H & C_{17}H) are shown multiplet peaks at 7.40–7.45 ppm and another two aromatic protons (C_{14}H & C_{16}H) are shown doublet peaks at 6.94, 6.92 ppm (Fig. 7 & 8) [51]. The four aromatic protons of the α-Tetralone moiety are shown at four different peaks. The C_1H proton has mulplet peaks at 7.33–7.37 ppm, the C_2H proton has doublet peaks at 7.47, 7.49 ppm, the C_3H proton has doublet peaks at 7.23, 7.25 ppm, and the C_4H proton has doublet peaks at 8.10, 8.12 ppm [38]. Two triplet peaks are shown in the ^{1}H NMR spectrum of the EBDN, which are attributed to two methylene protons (C_7H_2 & C_8H_2) of the α-Tetralone moiety. And finally, a characteristic singlet peak is shown at 7.84 ppm, which is assigned to methine (Ar-CH=C) proton (Fig. 7 & 8) [38].

3.2.3.2. ^{13}C NMR spectral charatcerization. In the ^{13}C NMR spectrum of the title compound EBDN, a peak is shown at 188.07 ppm, which is attributed to the carbonyl (C=O) group (Fig. 7 & 9). In the 4-ethoxybenzylidene moiety, the methyl carbon (C_{19}) is shown a peak at 14.98 ppm and methylene carbon (C_{18}) is shown a peak at 63.77 ppm [51]. Peaks for the four equivalent carbons are shown at 128.27 ppm (C_{12}), 131.97 ppm (C_{13} & C_{17}), 114.97 ppm (C_{14} & C_{16}), and 159.59 ppm (C_{15}). A peak at 136.97 ppm is shown for newly formed methine carbon (C_{11}).Two distinct peaks are shown for the two methylene carbons found in the α -tetralone moiety (Fig. 7 & 9). One is observed at 27.43 ppm (C_7) and another one is 29.01 ppm (C_8). Both C_6 and C_9 are shown a peak at 133.97 ppm. Peaks are shown for the five aromatic carbons at 128.45 for C_1, 133.62 for C_2, 127.16 for C_3, 128.35 for C_4 and 143.13 (**C_5**) [38,50,51].

Table 2
The geometrical parameters of the grown EBDN.

Bond length (Å)		Bond angles(°)		Dihedral angles [°]	
Atoms	Bond length	Atoms	Bond angle	Atoms	Dihedral angle
C(1)-C(6)	1.384(6)	C(6)-C(1)-C(2)	121.0(4)	C(6)-C(1)-C(2)-C(3)	−0.9(7)
C(1)-C(2)	1.389(5)	C(6)-C(1)-H(1)	119.5	C(1)-C(2)-C(3)-C(4)	0.2(7)
C(1)-H(1)	0.93	C(2)-C(1)-H(1)	119.5	C(2)-C(3)-C(4)-C(5)	0.3(7)
C(2)-C(3)	1.372(6)	C(3)-C(2)-C(1)	120.1(4)	C(3)-C(4)-C(5)-C(6)	−0.2(6)
C(2)-H(2)	0.93	C(3)-C(2)-H(2)	119.9	C(3)-C(4)-C(5)-C(10)	−179.1(4)
C(3)-C(4)	1.372(6)	C(1)-C(2)-H(2)	119.9	C(2)-C(1)-C(6)-C(5)	1.0(6)
C(3)-H(3)	0.93	C(2)-C(3)-C(4)	119.7(4)	C(2)-C(1)-C(6)-C(7)	180.0(4)
C(4)-C(5)	1.392(5)	C(2)-C(3)-H(3)	120.1	C(4)-C(5)-C(6)-C(1)	−0.4(6)
C(4)-H(4)	0.93	C(4)-C(3)-H(3)	120.1	C(10)-C(5)-C(6)-C(1)	178.4(4)
C(5)-C(6)	1.388(5)	C(3)-C(4)-C(5)	120.3(4)	C(4)-C(5)-C(6)-C(7)	−179.5(4)
C(5)-C(10)	1.485(5)	C(3)-C(4)-H(4)	119.8	C(10)-C(5)-C(6)-C(7)	−0.6(6)
C(6)-C(7)	1.493(5)	C(5)-C(4)-H(4)	119.8	C(1)-C(6)-C(7)-C(8)	144.6(4)
C(7)-C(8)	1.521(6)	C(6)-C(5)-C(4)	120.5(4)	C(5)-C(6)-C(7)-C(8)	−36.4(5)
C(7)-H(7A)	0.97	C(6)-C(5)-C(10)	120.3(3)	C(6)-C(7)-C(8)-C(9)	54.7(5)
C(7)-H(7B)	0.97	C(4)-C(5)-C(10)	119.1(4)	C(7)-C(8)-C(9)-C(11)	142.5(4)
C(8)-C(9)	1.500(5)	C(1)-C(6)-C(5)	118.2(4)	C(7)-C(8)-C(9)-C(10)	−38.4(5)
C(8)-H(8A)	0.97	C(1)-C(6)-C(7)	121.9(4)	C(6)-C(5)-C(10)-O(1)	−162.8(4)
C(8)-H(8B)	0.97	C(5)-C(6)-C(7)	119.8(4)	C(4)-C(5)-C(10)-O(1)	16.1(6)
C(9)-C(11)	1.334(5)	C(6)-C(7)-C(8)	110.9(4)	C(6)-C(5)-C(10)-C(9)	18.8(6)
C(9)-C(10)	1.490(5)	C(6)-C(7)-H(7A)	109.4	C(4)-C(5)-C(10)-C(9)	−162.3(4)
C(10)-O(1)	1.223(4)	C(8)-C(7)-H(7A)	109.4	C(11)-C(9)-C(10)-O(1)	2.9(6)
C(11)-C(12)	1.459(5)	C(6)-C(7)-H(7B)	109.4	C(8)-C(9)-C(10)-O(1)	−176.2(4)
C(11)-H(11)	0.93	C(8)-C(7)-H(7B)	109.4	C(11)-C(9)-C(10)-C(5)	−178.6(4)
C(12)-C(13)	1.390(5)	H(7A)-C(7)-H(7B)	108	C(8)-C(9)-C(10)-C(5)	2.2(5)
C(12)-C(17)	1.394(5)	C(9)-C(8)-C(7)	111.3(3)	C(10)-C(9)-C(11)-C(12)	−172.6(3)
C(13)-C(14)	1.380(5)	C(9)-C(8)-H(8A)	109.4	C(8)-C(9)-C(11)-C(12)	6.5(7)
C(13)-H(13)	0.93	C(7)-C(8)-H(8A)	109.4	C(9)-C(11)-C(12)-C(13)	34.4(6)
C(14)-C(15)	1.376(5)	C(9)-C(8)-H(8B)	109.4	C(9)-C(11)-C(12)-C(17)	−150.1(5)
C(14)-H(14)	0.93	C(7)-C(8)-H(8B)	109.4	C(17)-C(12)-C(13)-C(14)	0.4(6)
C(15)-O(2)	1.365(4)	H(8A)-C(8)-H(8B)	108	C(11)-C(12)-C(13)-C(14)	176.0(4)
C(15)-C(16)	1.385(5)	C(11)-C(9)-C(10)	117.9(3)	C(12)-C(13)-C(14)-C(15)	−0.3(6)
C(16)-C(17)	1.368(5)	C(11)-C(9)-C(8)	124.8(4)	C(13)-C(14)-C(15)-O(2)	−179.0(4)
C(16)-H(16)	0.93	C(10)-C(9)-C(8)	117.3(3)	C(13)-C(14)-C(15)-C(16)	0.8(6)
C(17)-H(17)	0.93	O(1)-C(10)-C(5)	121.0(3)	O(2)-C(15)-C(16)-C(17)	178.4(4)
C(18)-O(2)	1.421(5)	O(1)-C(10)-C(9)	121.8(3)	C(14)-C(15)-C(16)-C(17)	−1.4(6)
C(18)-C(19)	1.492(5)	C(5)-C(10)-C(9)	117.2(3)	C(15)-C(16)-C(17)-C(12)	1.6(6)
C(18)-H(18A)	0.97	C(9)-C(11)-C(12)	129.5(3)	C(13)-C(12)-C(17)-C(16)	−1.0(6)
C(18)-H(18B)	0.97	C(9)-C(11)-H(11)	115.2	C(11)-C(12)-C(17)-C(16)	−176.8(4)
C(19)-H(19A)	0.96	C(12)-C(11)-H(11)	115.2	C(14)-C(15)-O(2)-C(18)	−0.8(5)
C(19)-H(19B)	0.96	C(13)-C(12)-C(17)	117.0(4)	C(16)-C(15)-O(2)-C(18)	179.4(4)
C(19)-H(19C)	0.96	C(13)-C(12)-C(11)	123.4(4)	C(19)-C(18)-O(2)-C(15)	−176.7(4)
C(20)-C(25)	1.380(6)	C(17)-C(12)-C(11)	119.5(4)	C(25)-C(20)-C(21)-C(22)	−0.3(7)
C(20)-C(21)	1.384(6)	C(14)-C(13)-C(12)	121.6(4)	C(20)-C(21)-C(22)-C(23)	1.8(7)
C(20)-H(20)	0.93	C(14)-C(13)-H(13)	119.2	C(21)-C(22)-C(23)-C(24)	−2.1(7)
C(21)-C(22)	1.385(6)	C(12)-C(13)-H(13)	119.2	C(22)-C(23)-C(24)-C(25)	0.8(6)
C(21)-H(21)	0.93	C(15)-C(14)-C(13)	120.2(4)	C(22)-C(23)-C(24)-C(29)	−179.5(4)
C(22)-C(23)	1.375(5)	C(15)-C(14)-H(14)	119.9	C(21)-C(20)-C(25)-C(24)	−0.9(6)
C(22)-H(22)	0.93	C(13)-C(14)-H(14)	119.9	C(21)-C(20)-C(25)-C(26)	179.7(4)
C(23)-C(24)	1.389(5)	O(2)-C(15)-C(14)	124.7(4)	C(23)-C(24)-C(25)-C(20)	0.7(6)
C(23)-H(23)	0.93	O(2)-C(15)-C(16)	116.1(4)	C(29)-C(24)-C(25)-C(20)	−179.0(4)
C(24)-C(25)	1.398(5)	C(14)-C(15)-C(16)	119.3(4)	C(23)-C(24)-C(25)-C(26)	−180.0(4)
C(24)-C(29)	1.486(5)	C(17)-C(16)-C(15)	120.2(4)	C(29)-C(24)-C(25)-C(26)	0.4(6)
C(25)-C(26)	1.505(5)	C(17)-C(16)-H(16)	119.9	C(20)-C(25)-C(26)-C(27)	−144.2(4)
C(26)-C(27)	1.519(5)	C(15)-C(16)-H(16)	119.9	C(24)-C(25)-C(26)-C(27)	36.5(5)
C(26)-H(26A)	0.97	C(16)-C(17)-C(12)	121.8(4)	C(25)-C(26)-C(27)-C(28)	−55.4(4)
C(26)-H(26B)	0.97	C(16)-C(17)-H(17)	119.1	C(26)-C(27)-C(28)-C(30)	−139.3(4)
C(27)-C(28)	1.505(5)	C(12)-C(17)-H(17)	119.1	C(26)-C(27)-C(28)-C(29)	39.5(5)
C(27)-H(27A)	0.97	O(2)-C(18)-C(19)	108.3(4)	C(23)-C(24)-C(29)-O(3)	−14.3(6)
C(27)-H(27B)	0.97	O(2)-C(18)-H(18A)	110	C(25)-C(24)-C(29)-O(3)	165.3(4)
C(28)-C(30)	1.327(5)	C(19)-C(18)-H(18A)	110	C(23)-C(24)-C(29)-C(28)	162.5(3)
C(28)-C(29)	1.489(5)	O(2)-C(18)-H(18B)	110	C(25)-C(24)-C(29)-C(28)	−17.8(6)
C(29)-O(3)	1.224(4)	C(19)-C(18)-H(18B)	110	C(30)-C(28)-C(29)-O(3)	−7.9(6)
C(30)-C(31)	1.461(5)	H(18A)-C(18)-H(18B)	108.4	C(27)-C(28)-C(29)-O(3)	173.3(4)
C(30)-H(30)	0.93	C(18)-C(19)-H(19A)	109.5	C(30)-C(28)-C(29)-C(24)	175.3(4)
C(31)-C(32)	1.388(5)	C(18)-C(19)-H(19B)	109.5	C(27)-C(28)-C(29)-C(24)	−3.5(5)
C(31)-C(36)	1.396(5)	H(19A)-C(19)-H(19B)	109.5	C(29)-C(28)-C(30)-C(31)	174.4(4)
C(32)-C(33)	1.373(5)	C(18)-C(19)-H(19C)	109.5	C(27)-C(28)-C(30)-C(31)	−6.8(7)
C(32)-H(32)	0.93	H(19A)-C(19)-H(19C)	109.5	C(28)-C(30)-C(31)-C(32)	148.8(5)
C(33)-C(34)	1.383(5)	H(19B)-C(19)-H(19C)	109.5	C(28)-C(30)-C(31)-C(36)	−35.8(6)
C(33)-H(33)	0.93	C(15)-O(2)-C(18)	118.1(3)	C(36)-C(31)-C(32)-C(33)	1.5(6)
C(34)-O(4)	1.369(4)	C(25)-C(20)-C(21)	121.1(5)	C(30)-C(31)-C(32)-C(33)	177.3(4)
C(34)-C(35)	1.385(5)	C(25)-C(20)-H(20)	119.5	C(31)-C(32)-C(33)-C(34)	−2.1(6)

(*continued on next page*)

Table 2 (*continued*)

Bond length (Å)		Bond angles(°)		Dihedral angles [°]	
Atoms	Bond length	Atoms	Bond angle	Atoms	Dihedral angle
C(35)-C(36)	1.380(5)	C(21)-C(20)-H(20)	119.5	C(32)-C(33)-C(34)-O(4)	−178.3(4)
C(35)-H(35)	0.93	C(20)-C(21)-C(22)	119.8(4)	C(32)-C(33)-C(34)-C(35)	1.3(6)
C(36)-H(36)	0.93	C(20)-C(21)-H(21)	120.1	O(4)-C(34)-C(35)-C(36)	179.4(4)
C(37)-O(4)	1.425(5)	C(22)-C(21)-H(21)	120.1	C(33)-C(34)-C(35)-C(36)	−0.1(6)
C(37)-C(38)	1.504(6)	C(23)-C(22)-C(21)	119.6(4)	C(34)-C(35)-C(36)-C(31)	−0.4(6)
C(37)-H(37A)	0.97	C(23)-C(22)-H(22)	120.2	C(32)-C(31)-C(36)-C(35)	−0.3(6)
C(37)-H(37B)	0.97	C(21)-C(22)-H(22)	120.2	C(30)-C(31)-C(36)-C(35)	−175.9(4)
C(38)-H(38A)	0.96	C(22)-C(23)-C(24)	120.8(4)	C(33)-C(34)-O(4)-C(37)	−176.5(4)
C(38)-H(38B)	0.96	C(22)-C(23)-H(23)	119.6	C(35)-C(34)-O(4)-C(37)	3.9(6)
C(38)-H(38C)	0.96	C(24)-C(23)-H(23)	119.6	C(38)-C(37)-O(4)-C(34)	171.6(4)
		C(23)-C(24)-C(25)	119.7(4)		
		C(23)-C(24)-C(29)	120.2(4)		
		C(25)-C(24)-C(29)	120.1(3)		
		C(20)-C(25)-C(24)	118.9(4)		
		C(20)-C(25)-C(26)	122.1(4)		
		C(24)-C(25)-C(26)	119.0(4)		
		C(25)-C(26)-C(27)	111.6(4)		
		C(25)-C(26)-H(26A)	109.3		
		C(27)-C(26)-H(26A)	109.3		
		C(25)-C(26)-H(26B)	109.3		
		C(27)-C(26)-H(26B)	109.3		
		H(26A)-C(26)-H(26B)	108		
		C(28)-C(27)-C(26)	111.0(3)		
		C(28)-C(27)-H(27A)	109.4		
		C(26)-C(27)-H(27A)	109.4		
		C(28)-C(27)-H(27B)	109.4		
		C(26)-C(27)-H(27B)	109.4		
		H(27A)-C(27)-H(27B)	108		
		C(30)-C(28)-C(29)	117.5(3)		
		C(30)-C(28)-C(27)	125.8(3)		
		C(29)-C(28)-C(27)	116.6(3)		
		O(3)-C(29)-C(24)	119.6(3)		
		O(3)-C(29)-C(28)	122.0(4)		
		C(24)-C(29)-C(28)	118.3(3)		
		C(28)-C(30)-C(31)	129.6(3)		
		C(28)-C(30)-H(30)	115.2		
		C(31)-C(30)-H(30)	115.2		
		C(32)-C(31)-C(36)	116.8(4)		
		C(32)-C(31)-C(30)	119.6(3)		
		C(36)-C(31)-C(30)	123.4(3)		
		C(33)-C(32)-C(31)	122.3(4)		
		C(33)-C(32)-H(32)	118.8		
		C(31)-C(32)-H(32)	118.8		
		C(32)-C(33)-C(34)	119.7(4)		
		C(32)-C(33)-H(33)	120.1		
		C(34)-C(33)-H(33)	120.1		
		O(4)-C(34)-C(33)	115.6(4)		
		O(4)-C(34)-C(35)	124.8(4)		
		C(33)-C(34)-C(35)	119.7(4)		
		C(36)-C(35)-C(34)	119.7(4)		
		C(36)-C(35)-H(35)	120.2		
		C(34)-C(35)-H(35)	120.2		
		C(35)-C(36)-C(31)	121.8(4)		
		C(35)-C(36)-H(36)	119.1		
		C(31)-C(36)-H(36)	119.1		
		O(4)-C(37)-C(38)	106.9(4)		
		O(4)-C(37)-H(37A)	110.3		
		C(38)-C(37)-H(37A)	110.3		
		O(4)-C(37)-H(37B)	110.3		
		C(38)-C(37)-H(37B)	110.3		
		H(37A)-C(37)-H(37B)	108.6		
		C(37)-C(38)-H(38A)	109.5		
		C(37)-C(38)-H(38B)	109.5		
		H(38A)-C(38)-H(38B)	109.5		
		C(37)-C(38)-H(38C)	109.5		
		H(38A)-C(38)-H(38C)	109.5		
		H(38B)-C(38)-H(38C)	109.5		
		C(34)-O(4)-C(37)	117.9(3)		

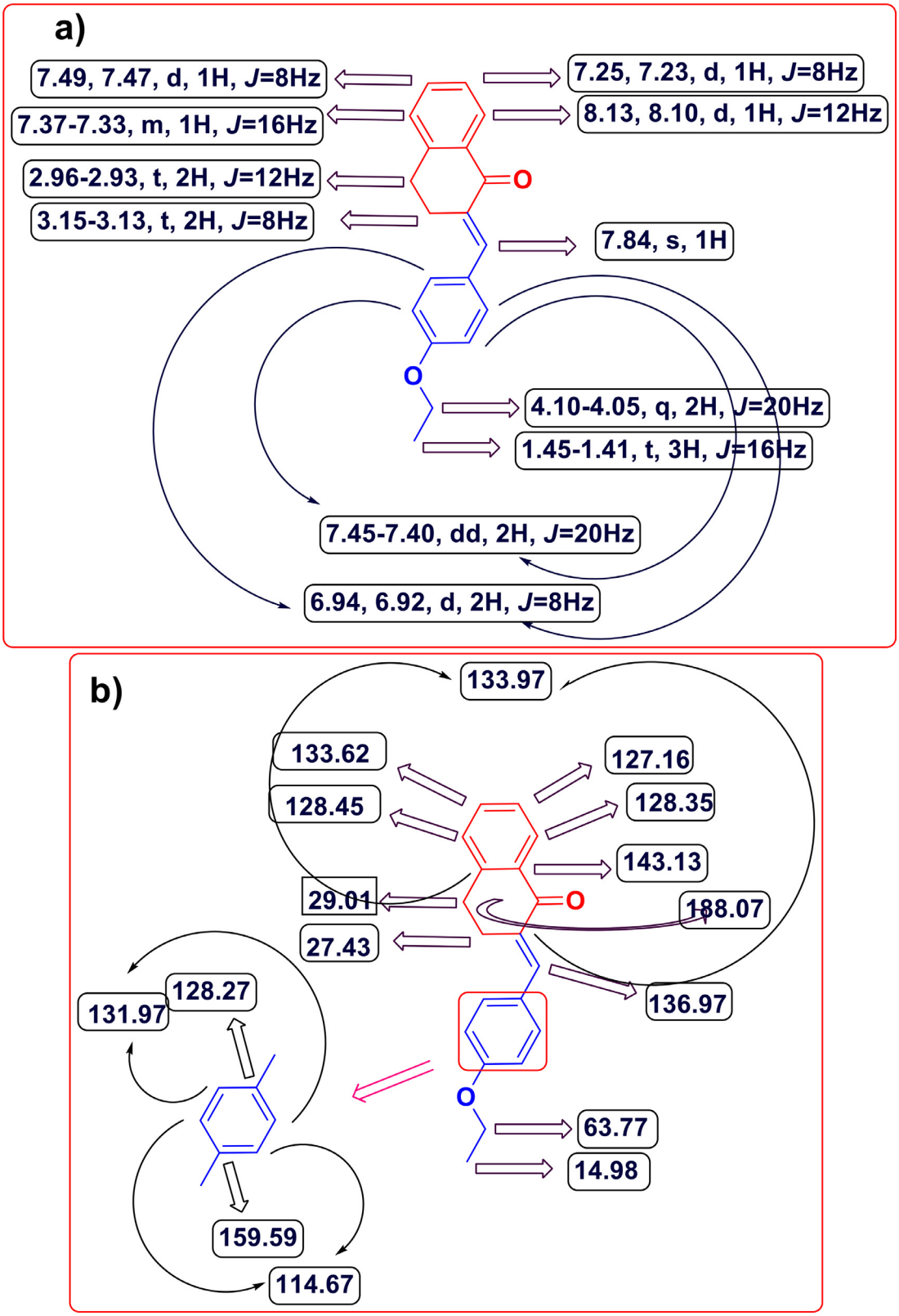

Fig. 7. ^{1}H NMR and ^{13}C NMR spectral data representation of the grown EBDN.

3.2.4. Thermal studies

Thermal gravimetric (TG) and Differential thermal analysis (DTA) were performed on the grown crystal in the nitrogen atmosphere. The studies were embedded in the temperature range of 30–450 °C with a slow heating rate of 20 °C/min. Initially, 2.078 mg of the sample weighing was taken for the measurement, and the thermogram is illustrated in Fig. 10. Because there is no weight loss in the TG curve at temperatures up to 238 °C, it is clear that the crystal is thermally stable. The small exothermic peak exists at 141 °C (The melting point of the EBDN is 141–142 °C) in

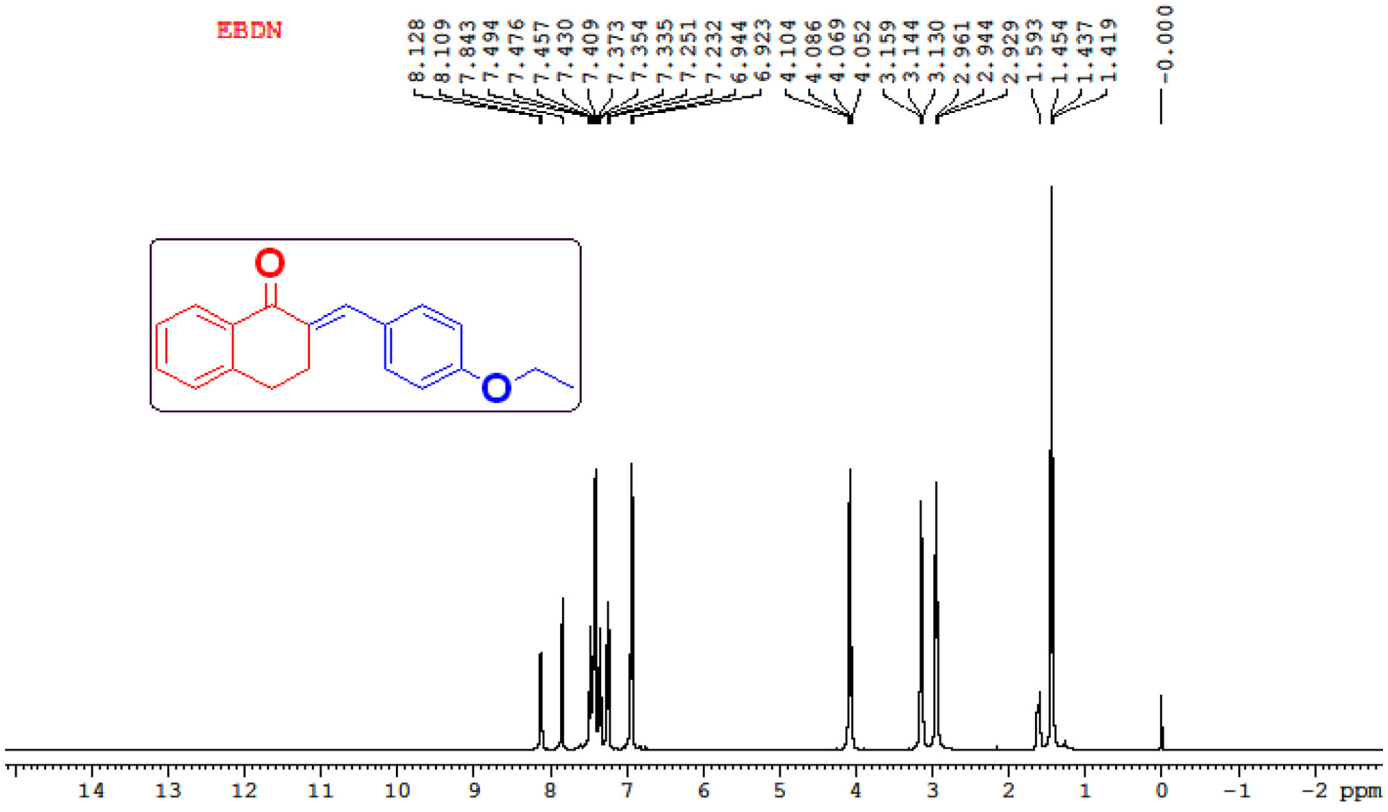

Fig. 8. ^{1}H NMR spectrum of the grown EBDN.

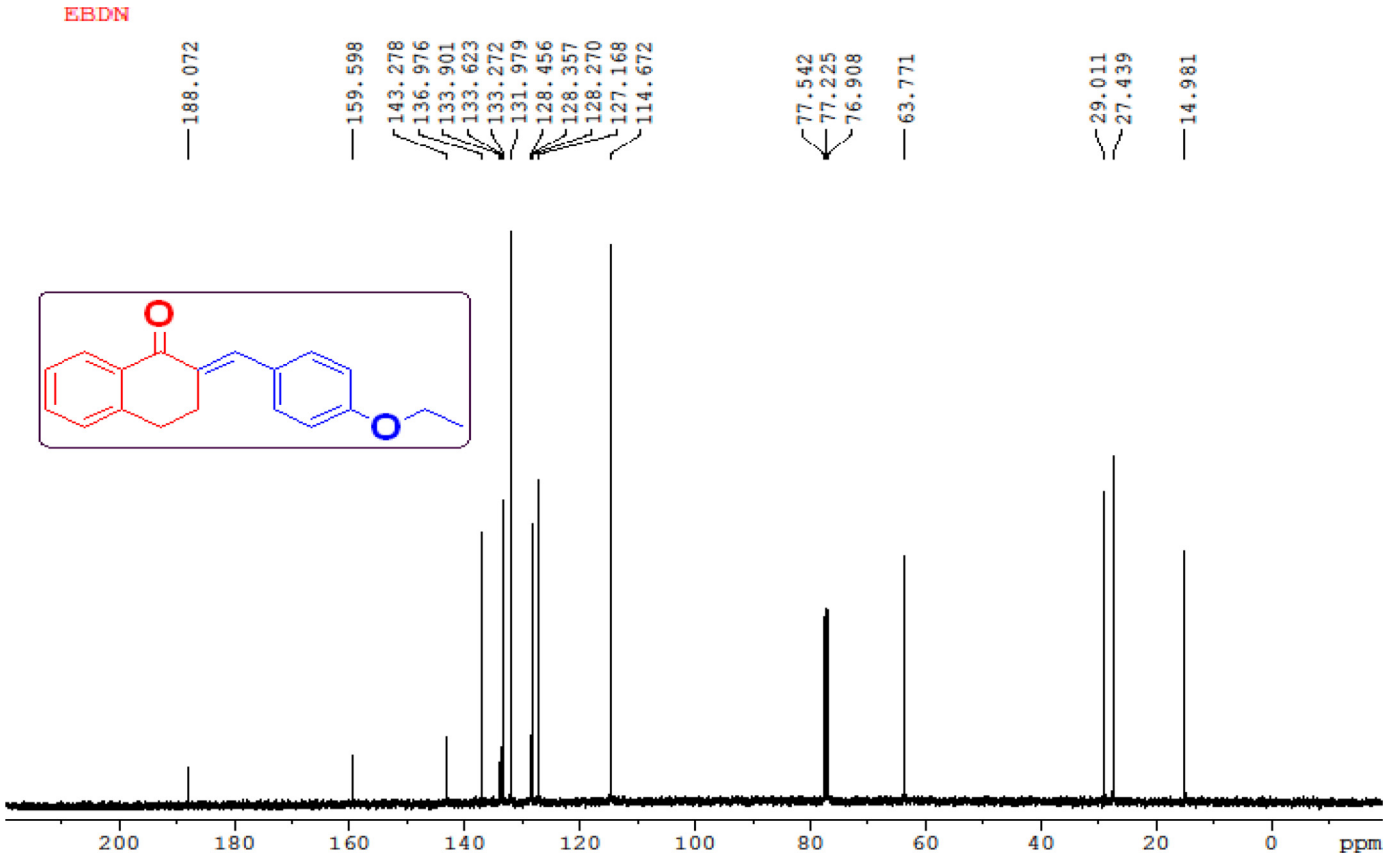

Fig. 9. ^{13}C NMR spectra spectrum of the grown EBDN.

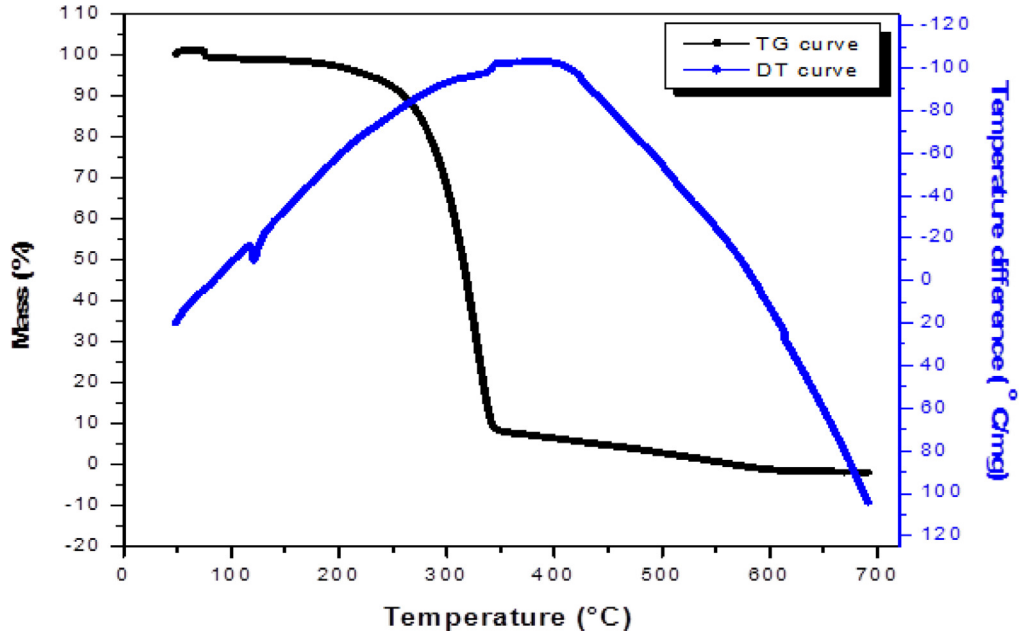

Fig. 10. TG and DTA curve of grown EBDN.

Table 3
FT-IR data and functional group confirmation of grown EBDN crystal.

S. No.	Vibrational frequency (ν, cm^{-1})	Vibrational assignment(s)
1	3068, *vw*	C-H
2	2960, *vs*	C–H
3	1675, *s*	C=O
4	1599, *vs*	C=C/C=O
5	1508, *vs*	C=C
6	1253,*vs*	C-O
7	977, *s*	C–H
8	838, *s*	C-H
9	728, *s*	C–H
10	541, *s*	C-H

the DTA curve (Fig. 10) confirms the melting point of the crystal. The weight loss begins gradually above 238 °C and becomes almost steep until it reaches 365 °C, when 95% of the material decomposes into a gaseous state. The two endothermic peaks in the DTA curve at 335 °C and 352 °C correspond to energy absorbed by the material to decompose in the temperature range of 238 °C-365 °C. There is no weight loss observed above 365 °C.

3.2.5. Photoluminescence studies

The FP-6500 Spectro-fluorometer was used to analyze the photoluminescence (PL) of the grown crystal at an optical excitation wavelength of 375 nm, and spectra were recorded in the range 350–700 nm. The recorded PL spectrum is shown in Fig. 11. Strong emission in the blue range is observed with two peaks at 452 nm and 464 nm for this excitation. The luminescence property of the chalcone derivatives can be used effectively in the field of design of optoelectronic devices and laser applications.

3.2.6. Mechanical studies

The structure and composition of the crystalline solids are inviolably related to the mechanical hardness. The EBDN crystal's microhardness was measured using a Leitz-Wetzlar Vickers' microhardness tester equipped with a diamond pyramidal indenter and attached to an optical microscope.Microhardness studies were performed on **EBDN** crystal for loads in the range of 10–60 g. From Fig. 12, it is observed that Vicker's hardness (H_v) number increases

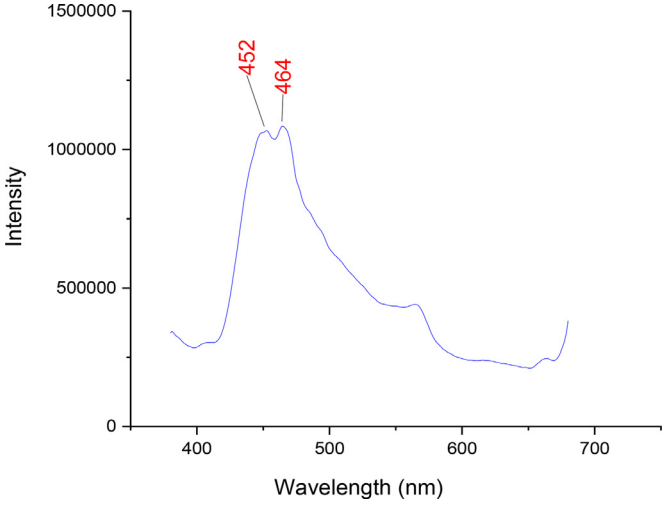

Fig. 11. Photoluminescence graph of grown EBDN.

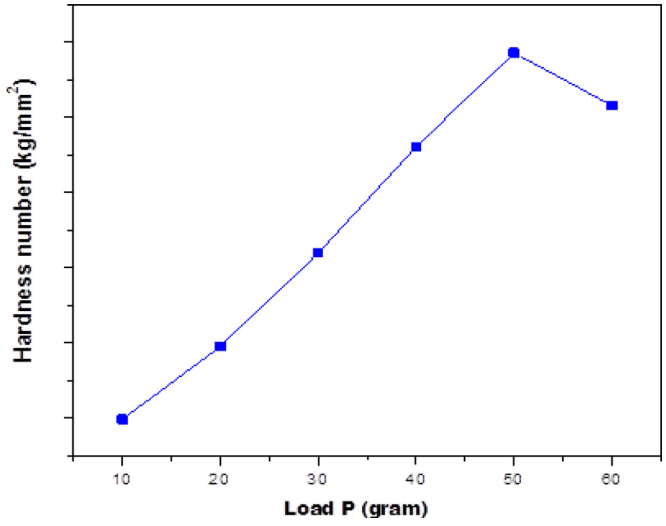

Fig. 12. Plot of Vickers' hardness (H_v) against load (P) of EBDN crystal.

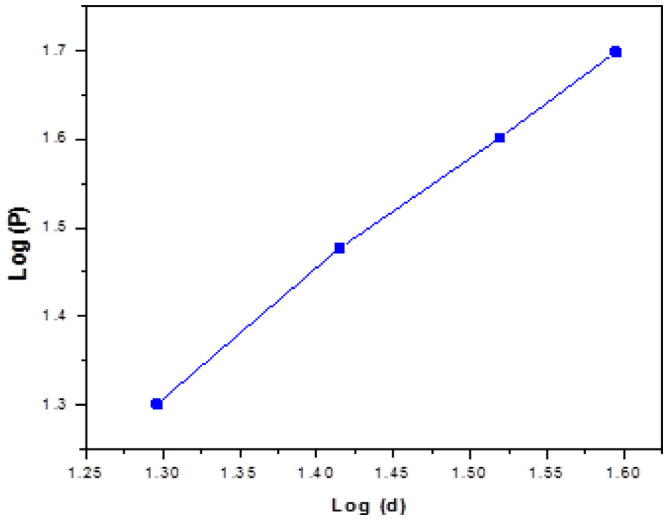

Fig. 13. Plot of log d vs log P of EBDN crystal.

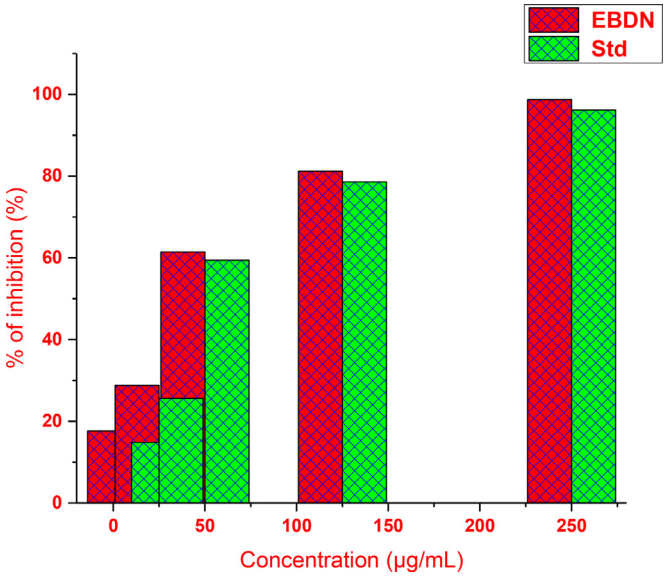

Fig. 14. Anti-inflammatory activity of EBDN.

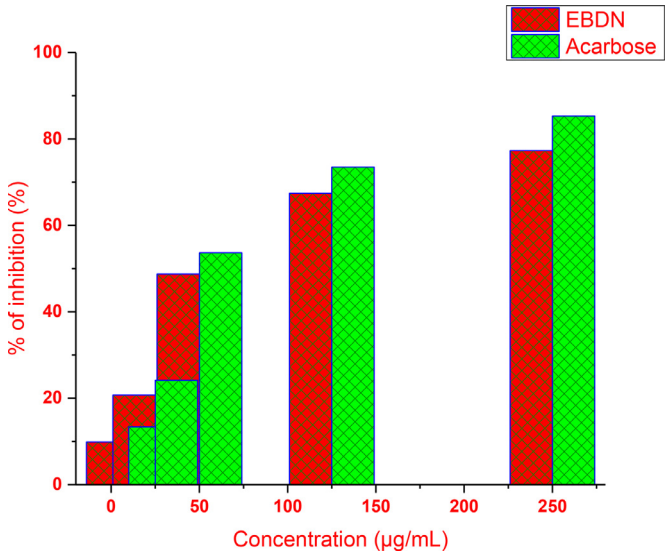

Fig. 15. Anti-diabetic activity of grown EBDN.

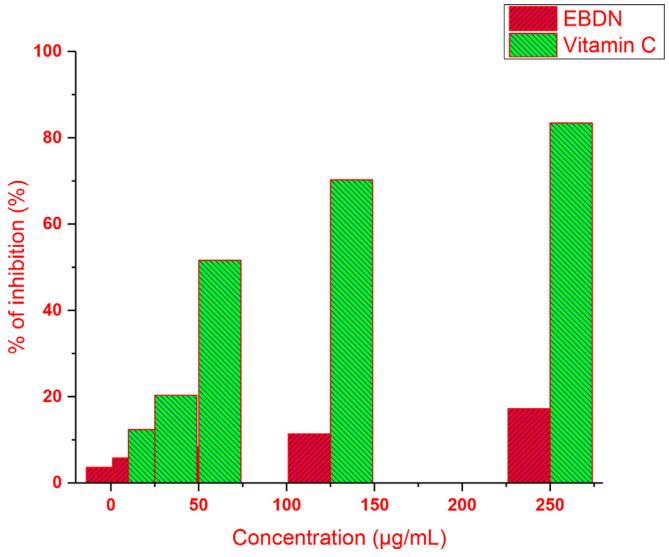

Fig. 16. Anti-oxidant activity of grown EBDN.

initially with load up to 50 g and cracks were observed beyond 50 g. This type of load variation of hardness is termed as the reverse indentation size effect. At low loads, the indenter penetrates only the top surface layers, generating dislocations, which results in the increase of hardness in this region. The load independence to hardness at higher loads can be attributed to the mutual interaction or rearrangement of dislocations. The relation between load and the size of indentation can be correlated using Meyer's law, $P = k_1 d^n$, where k_1 is a constant and 'n' is the Meyer's index. The slope of log P versus log d gives the work hardening coefficient (n) and it is found to be 1.36, which indicates that **EBDN** crystal belongs to the hard material category (Fig. 13).

3.2.7. Biological evaluation

The grown **EBDN** was screened for its anti-inflammatory (see Section 3.2.7.1.), anti-diabetic (see Section 3.2.7.2.) and antioxidant (see Section 3.2.7.3.) activities and percentage of inhibition are shown in Figs. 14–16 and its results are summarized in Table 4.

3.2.7.1. Anti-inflammatory activity of grown EBDN. The grown **EBDN** was screened for its anti-inflammatory activity in five different concentrations (10, 25, 50, 125 & 250 μg/mL) and the percentage of inhibition (%) is summarized in Table 4 and shown in Fig. 14. Diclofenac sodium was used as a standard drug for this present work. The 10 µg/mL concentration of grown **EBDN** was shown 17.62% of inhibition of anti-inflammatory activity. The stan-

Table 4
Anti-inflammatory, anti-diabetic and anti-oxidant activity of grown EBDN.

Compound	Percentage of inhibition (%)					IC_{50} (µg/mL)
	Concentration (µg/mL)					
	10	25	50	125	250	
Anti-inflammatory activity						
EBDN	17.62	28.79	61.43	81.19	98.71	133.95
*Diclofenac sodium**	14.82	25.63	59.44	78.59	96.22	150.66
Anti-diabetic activity						
EBDN	9.89	20.74	48.73	67.42	77.31	221.87
*Acarbose**	13.37	24.15	53.67	73.48	85.32	181.95
Anti-oxidant activity						
EBDN	3.61	5.80	8.37	11.41	17.22	1736.14
*Vitamin C**	12.42	20.36	51.62	70.28	83.44	198.96

* Standard drug.

Table 5
Protein-ligand binding interactions of EBDN with 6yb7.

Compound	Binding energy (Kcal/mol)	Number of hydrogen bonds	Inhibition constant (μM)	Interacting residues (H-A distance)
EBDN	−7.25	4	4.85	THR26 (3.03 Å), CYS145 (3.68 Å), GLU166 (3.65 Å), GLU166 (3.04 Å)

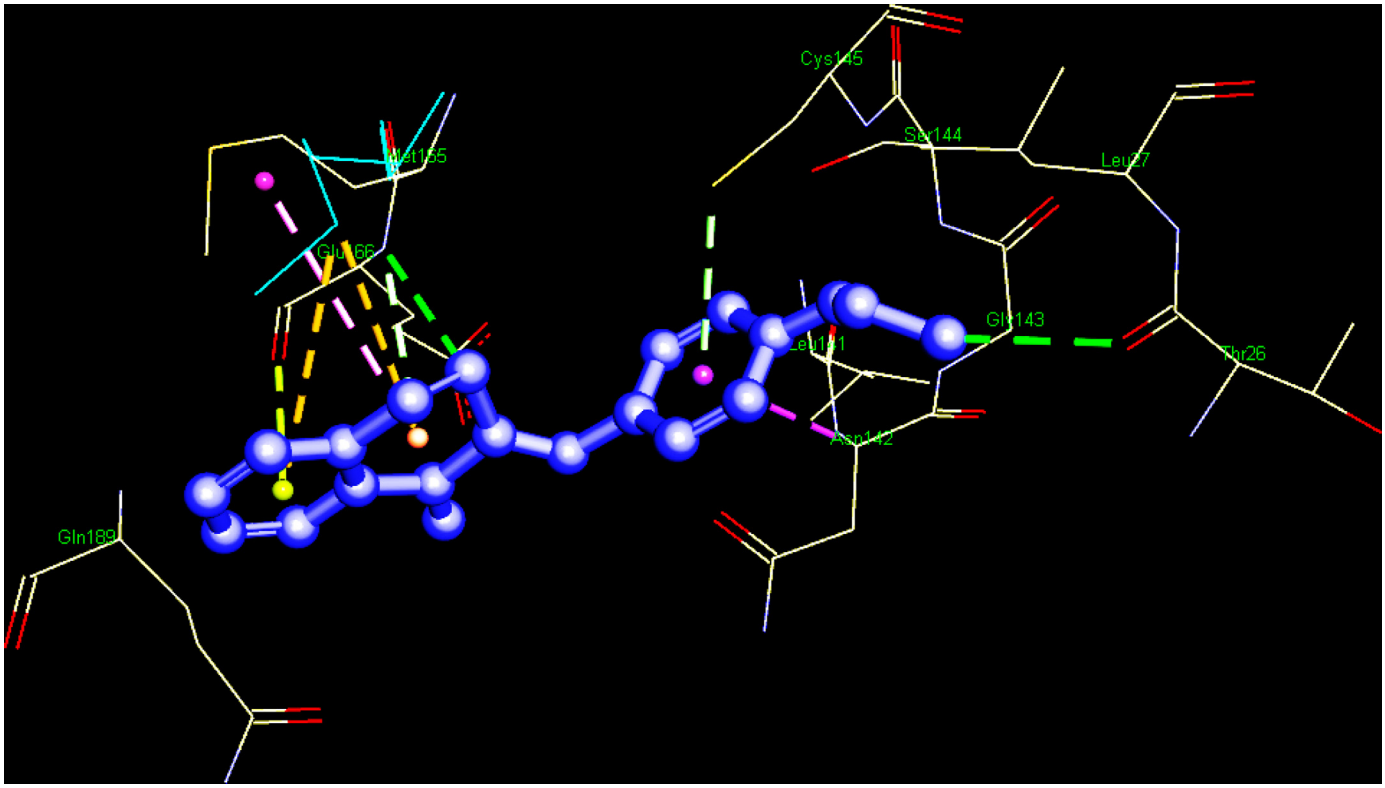

Fig. 17. Protein-Ligand binding interaction of EBDN in the active site pocket of 6yb7.

dard drug was shown 14.82% of inhibition. The grown **EBDN** and standard drug were shown 28.79 and 25.63%, 61.43 and 59.44%, 81.19 and 78.59% and, 98.71 and 96.22% in the concentration of 25, 50, 125 and 250 μg/mL respectively. When compared to the standard drug (IC_{50} value 150.66 μg/mL), the percentage of inhibition of grown EBDN (IC_{50} value 133.95 μg/mL) was excellent, and its results were strongly cleared as an admirable anti-inflammatory agent.

3.2.7.2. Antidiabetic activity of grown EBDN. The grown **EBDN** was screened for its anti-diabetic activity in five different concentrations (10, 25, 50, 125 & 250 μg/mL) and the percentage of inhibition (%) is summarized in Table 4 and shown in Fig. 15. Acarbose was used as a standard drug for this present work. The anti-diabetic activity of grown EBDN was inhibited by 9.89% at 10 g/mL concentration. The standard drug was shown 13.37% of inhibition. The grown **EBDN** and standard drug were shown 20.74 and 24.15%, 48.73 and 53.67%, 67.42 and 73.48% and, 77.31 and 85.32% in the concentration of 25, 50, 125 and 250 μg/mL respectively. The percentage of inhibition of grown EBDN (IC_{50} value 221.87 μg/mL) was very close to that of the standard drug (IC_{50} value 181.95 μg/mL), and its results were strongly supported as an excellent anti-inflammatory agent.

3.2.7.3. Antioxidant activity of grown EBDN. The grown **EBDN** was screened for its anti-oxidant activity in five different concentrations (10, 25, 50, 125 & 250 μg/mL) and the percentage of inhibition (%) is summarized in Table 4 and shown in Fig. 16. Vitamin C was used as a standard drug for this present work. The 10 μg/mL concentration of grown **EBDN** was shown 3.61% of inhibition of anti-oxidant activity. The standard drug was shown 12.42% of inhibition. The grown **EBDN** and standard drug were shown 5.80 and 20.36%, 8.37 and 51.62%, 11.41 and 70.28% and, 17.22 and 83.44% in the concentration of 25, 50, 125 and 250 μg/mL respectively. The% of inhibition of grown **EBDN** (IC_{50} value 1736.14 μg/mL) was moderate activity compared to the standard drug (IC_{50} value 198.96 μg/mL) and its results indicate the compound **EBDN** should be further modified structurally.

3.2.7.4. Protein-ligand binding interaction of EBDN with 6yb7. The binding energy, number of hydrogen bond interactions, inhibition constant and interacting amino acid residues were summarized in Table 5. The binding energy of the synthesized chalcone compound EBDN is −7.25 Kcal/mol [39–45]. The EBDN has shown strong four hydrogen bond (H-bond) interaction with targeted SARS-CoV-2 main protease (6yb7). The first H-bond interaction is shown with the amino acid residue of THR26, which is due to the H-A distance of 3.03 Å (Table 5, Fig. 17). The second H-bond interaction is shown with CYS145 and the H-A distance is 3.68 Å (Table 5, Fig. 17). Both third and fourth H-bond interactions were shown with the GLU166 amino acid residue of the SARS CoV-2 main protease and the H-A distances are 3.65 and 3.04 Å (Table 5, Fig. 17) respectively. Among them, four H-bond interactions, H-A distance of two interactions are shown a strong binding with SARS CoV-2 main protease, which is due to THR26 (3.03 Å) and GLU166 (3.04 Å) [43].

4. Conclusion

To summarize, we have presented in this paper, the synthesis and crystal growth (2E)-2-(4-ethoxybenzylidene)-3,4-dihydro-2H-naphthalen-1-one single crystal (EBDN) in excellent yield under very mild conditions. It has been fully characterized by cyrstallographic and spectral analysis. The synthesized EBDN was successfully screened for its anti-inflammatory, anti-diabetic and anti-oxidant activities. Its results have also been shown as an excellent anti-inflammatory as well as anti-diabetic agents and moderate anti-oxidant activity. The EBDN's binding interactions and binding affinity with SARS-CoV-2 are also investigated, and the results show a very good binding with the targeted main protease (6yb7).

Declaration of Competing Interest

The authors declare that they have no known competing financial interests or personal relationships that could have appeared to influence the work reported in this paper.

CRediT authorship contribution statement

N. Afsar: Conceptualization, Data curation, Formal analysis, Investigation, Validation, Writing – original draft. **D. Reuben Jonathan:** Conceptualization, Formal analysis, Investigation, Visualization. **B.K. Revathi:** Methodology, Software. **Dhurairaj Satheesh:** Data curation, Formal analysis, Validation, Visualization. **S. Manivannan:** Conceptualization, Supervision, Writing – review & editing.

References

[1] B. Zhou, C. Xing, Diverse molecular targets for chalcones with varied bioactivities, Med. Chem. 5 (2015) 388–404.
[2] D.I. Batovska, I.T. Todorova, Trends in utilization of the pharmacological potential of chalcones, Curr. Clin. Pharmacol. 5 (2010) 1–29.
[3] N.K. Sahu, S.S. Balbhadra, J. Choudhary, D.V. Kohli, Exploring pharmacological significance of chalcone scaffold: a review, Curr. Med. Chem. 19 (2012) 209–225.
[4] P. Singh, A. Anand, V. Kumar, Recent developments in biological activities of chalcones: a mini review, Eur. J. Med. Chem. 85 (2014) 758–777.
[5] C. Karthikeyan, N.S. Moorthy, S. Ramasamy, U. Vanam, E. Manivannan, D. Karunagaran, P. Trivedi, Advances in chalconeswith anticancer activities, Recent Pat. Anti-Cancer Drug Discov. 10 (2015) 97–115.
[6] S. Sebti, A. Solhy, A. Smahi, A. Kossir, H. Oumimoun, Dramatic activity enhancement of natural phosphate catalyst by lithium nitrate. An efficient synthesis of chalcones, Catal. Commun. 3 (2002) 335–339.
[7] M.N. Arshad, A.-A.M. Al-Dies, A.M. Asiri, M. Khalid, A.S. Birinji, K.A. Al-Amry, A. Ataualpa, C. Braga, J. Mol. Struct. 1141 (2017) 142–156.
[8] A. Mascarello, L.D. Chiaradia, J. Vernal, A. Villarino, R.V. Guido, P. Perizzolo, V. Poirier, D. Wong, P.G. Martins, R.J. Nunes, R.A. Yunes, A.D. Andricopulo, Y. Av-Gay, H. Terenzi, Inhibition of *Mycobacterium tuberculosis* tyrosine phosphatase PtpA by synthetic chalcones: kinetics, molecular modeling, toxicity and effect on growth, Bioorg. Med. Chem. 18 (11) (2010) 3783–3789.
[9] V. Tomar, G. Bhattacharjee, Kamaluddin, S. Rajakumar, K. Srivastava, S.K. Puri, Synthesis of new chalcone derivatives containing acridinyl moiety with potential antimalarial activity, Eur. J.Med. Chem. 45 (2) (2010) 745–751.
[10] S.U.F. Rizvi, H.L. Siddiqui, M. Johns, M. Detorio, R.F. Schinazi, Anti-HIV-1 and cytotoxicity studies of piperidyl-thienyl chalcones and their 2-pyrazoline derivatives, Med. Chem. Res. 21 (21) (2012) 3741–3749.
[11] M.I. Abdullah, A. Mahmood, M. Madni, S. Masood, M. Kashif, Synthesis, characterization, theoretical, anti-bacterial and molecular docking studies of quinoline based chalcones as a DNA gyrase inhibitor, Bioorg. Chem. 54 (2014) 31–37.
[12] D.K. Mahapatra, S.K. Bharti, V. Asati, Anti-cancer chalcones: structural and molecular target perspectives, Eur. J. Med. Chem. 98 (2015) 69–114.
[13] L. Wang, G. Chen, X. Lu, S. Wang, S. Han, Y. Li, G. Ping, X. Jiang, H. Li, J. Yang, C. Wu, Novel chalcone derivatives as hypoxiainducible factor (HIF)-1 inhibitor: synthesis, anti-invasive and antiangiogenic properties, Eur. J. Med. Chem. 89 (2015) 88–97.
[14] E. Winter, C. Locatelli, A. Di Pietro, T.B. Creczynski-Pasa, Recent trends of chalcones potentialities as antiproliferative and antiresistance agents, Anti-Cancer Agents Med. Chem. 15 (5) (2015) 592–604.
[15] H.-L. Qin, Z.-P. Shang, I. Jantan, O.U. Tan, M.A. Hussain, M. Sher, S.N.A. Bukhari, Molecular docking studies and biological evaluation of chalcone based pyrazolines as tyrosinase inhibitors and potential anticancer agents, RSC Adv. 5 (2015) 46330–46338.
[16] R.B. Birari, S. Gupta, C.G. Mohan, K.K. Bhutani, Antiobesity and lipid lowering effects of glycyrrhizachalcones: experimental and computational studies, Phytomedicine 18 (8–9) (2011) 795–801.
[17] S. Kantevari, D. Addla, P.K. Bagul, B. Sridhar, S.K. Banerjee, Synthesis and evaluation of novel 2-butyl-4-chloro-1-methylimidazole embedded chalcones and pyrazoles as angiotensin converting enzyme (ACE) inhibitors, Bioorg. Med. Chem. 19 (16) (2011) 4772–4781.
[18] K.V. Sashidhara, G.R. Palnati, R. Sonkar, S.R. Avula, C. Awasthi, G. Bhatia, Coumarinchalcone fibrates: a new structural class of lipid lowering agents, Eur. J. Med. Chem. 64 (2013) 422–431.
[19] D.K. Mahapatra, V. Asati, S.K. Bharti, Chalcones and their role in management of diabetes mellitus: structural and pharmacological perspectives, Eur. J. Med. Chem. 92 (2015) 839–865.
[20] A. Gomez-Rivera, H. Aguilar-Mariscal, N. Romero-Ceronio, L.F. Roa-de la Fuente, C.E. Lobato-Garcia, Synthesis and anti-inflammatory activity of three nitro chalcones, Bioorg. Med. Chem. Lett. 23 (2013) 5519–5522.
[21] N. Aoki, M. Muko, E. Ohta, S. Ohta, C-Geranylated chalcones from the stems of Angelica keiskei with superoxide-scavenging activity, J. Nat. Prod. 71 (7) (2008) 1308–1310.
[22] S.N. Bukhari, Y. Tajuddin, V.J. Benedict, K.W. Lam, I. Jantan, J. Jalil, M. Jasamai, Synthesis and evaluation of chalcone derivatives as inhibitors of neutrophils' chemotaxis, phagocytosis and production of reactive oxygen species, Chem. Biol. Drug Des. 83 (2) (2014) 198–206.
[23] S.N. Bukhari, X. Zhang, I. Jantan, H.L. Zhu, M.W. Amjad, V.H. Masand, Synthesis, molecular modeling, and biological evaluation of novel 1, 3-diphenyl-2-propen-1-one based pyrazolines as anti-inflammatory agents, Chem. Biol. Drug Des. 85 (6) (2015) 729–742.
[24] J.R. Dimmock, D.W. Elias, M.A. Beazely, N.M. Kandepu, Bioactivities of chalcones, Curr. Med. Chem. 6 (12) (1999) 1125–1149.
[25] N.K. Sahu, S.S. Balbhadra, J. Choudhary, D.V. Kohli, Exploring pharmacological significance of chalcone scaffold: a review, Curr. Med. Chem. 19 (2) (2012) 209–225.
[26] D.I. Batovska, I.T. Todorova, Trends in utilization of the pharmacological potential of chalcones, Curr. Clin. Pharmacol. 5 (2010) 1–29.
[27] S. Arora, A. Pareek, N. Agrawal, B. Nagori, Synthesis and antimicrobial activity of indazoline tetralone, Int. J. Res. Pharm. Chem. 3 (2013) 797–802.
[28] H. Shih, L. Deng, C.J. Carrera, S. Adachi, H.B. Cottam, D.A. Carson, Rational design, synthesis and structure–activity relationships of antitumor (E)-2-benzylidene-1-tetralones and (E)-2-benzylidene-1-indanones, Bioorg. Med. Chem. Lett. 10 (2000) 487–490.
[29] L.J. Legoabe, M.M. Van der Walt, G. Terre'Blanche, Evaluation of 2-benzylidene-1-tetralone derivatives as antagonists of A1 and A2A adenosine receptors, Chem. Biol. Drug. Des. 91 (2018) 234–244.
[30] H.D. Janse van Rensburg, G. Terre'Blanche, M.M. van der Walt, L.J. Legoabe, 5-Substituted 2-benzylidene-1-tetralone analogues as A 1 and/or A 2A antagonists for the potential treatment of neurological conditions, Bioorganic Chem. 74 (2017) 251–259.
[31] H. Shih, L. Deng, C.J. Carrera, S. Adachi, H.B. Cottam, D.A. Carson, Rational design, synthesis and structure–activity relationships of antitumor (E)-2-benzylidene-1-tetralones and (E)-2-benzylidene-1-indanones, Bioorg. Med. Chem. Lett. 10 (2000) 487–490.
[32] L.J. Legoabe, M.M. Van der Walt, G. Terre'Blanche, Evaluation of 2-benzylidene-1-tetralone derivatives as antagonists of A1 and A2A adenosine receptors, Chem. Biol. Drug. Des. 91 (2018) 234–244.
[33] H.D. Janse van Rensburg, G. Terre'Blanche, M.M. van der Walt, L.J. Legoabe, 5-Substituted 2-benzylidene-1-tetralone analogues as A 1 and/or A 2A antagonists for the potential treatment of neurological conditions, Bioorganic Chem 74 (2017) 251–259.
[34] R. Kamakshi, S. Swarna Latha, B.S.R. Reddy, An efficient synthesis of bioactive fluorescent benzylidine tetralones, Indian J. Chem. Sect. B Org. Chem. Incl. Med. Chem. 49 (2010) 944–947.
[35] P. Perješi, J. Linnanto, E. Kolehmainen, E. O¨sz, E. Virtanen, E-2-Benzylidenebenzocycloalkanones. IV. Studies on transmission of substituent effects on 13C NMR chemical shifts of E-2-(X-benzylidene)-1-tetralones, and -benzosuberones. Comparison with the 13C NMR data of chalcones and E-2-(X-benzylidene)-1-indanones, J. Mol. Struct. 740 (2005) 81–89.
[36] M. Štefanišinová, V. Tomečková, M. Kožurková, A. Ostró, M. Mareková, Study of DNA interactions with cyclic chalcone derivatives by spectroscopic techniques, Spectrochim. Acta Part A 81 (1) (2011) 666–671.
[37] V. Tomečková, J. Guzy, J. Kušnír, K. Fodor, M. Mareková, Z. Chavková, P. Perjési, Comparison of the effects of selected chalcones, dihydrochalcones and some cyclic flavonoids on mitochondrial outer membrane determined by fluorescence spectroscopy, J. Biochem. Biophys. Methods 69 (1–2) (2006) 143–150.
[38] P. Katila, A. Shrestha, A. Shrestha Ritina Shrestha, P.-H. Park, E. SeokLee, Introduction of amino moiety enhances the inhibitory potency of 1-tetralone chalcone derivatives against LPS-stimulated reactive oxygen species production in RAW 264.7 macrophages, Bioorg. Chem. 87 (2019) 495–505.
[39] M.R. Rameshkumar, P. Indu, N. Arunagirinathan, B. Venkatadri, H.A. El-Serehy, A. Ahmad, Computational selection of flavonoid compounds as inhibitors against SARS-CoV-2 main protease, RNA-dependent RNA polymerase and spike proteins: a molecular docking study, Saudi J. Biol. Sci. 28 (2021) 448–458.
[40] T. Erdogan, DFT, molecular docking and molecular dynamics simulation studies on some newly introduced natural products for their potential use against SARS-CoV-2, J. Mol. Struct. 1242 (2021) 130733 Available online.

[41] R.K. Mohapatra, L. Perekhoda, M. Azam, M. Suleiman, A.K. Sarangi, A. Semenets, et al., Computational investigations of three main drugs and its comparison with synthesized compounds as potent inhibitors of SARS-CoV-2 main protease (M(pro)): DFT, QSAR, molecular docking, and in silico toxicity analysis, J. King Saud. Univ. Sci. 33 (2) (2020) 101315.
[42] S. Ercan, E. Çınar, A molecular docking study of potential inhibitors and repurposed drugs against SARS-CoV-2 main protease enzyme, J. Indian Chem. Soc. 98 (2021) 100041.
[43] D. Satheesh, A. Rajendran, K. Chithra, Protein-ligand binding interactions of imidazolium salts with SARS CoV-2, Heliyon 6 (2020) e05544.
[44] B.G. Vijayakumar, D. Ramesh, A. Joji, J.J. Prakasan, T. Kannan, In silico pharmacokinetic and molecular docking studies of natural flavonoids and synthetic indole chalcones against essential proteins of SARS-CoV-2, Eur. J. Pharmacol. 886 (2020) 173448.
[45] J. Syahri, B.A. Nurohmah, E. Yuanita, Effectivity of Remdesivir and some compounds as therapeutic potential drugs for anti-SARS-CoV-2: in silico study, Jordan J. Pharm. Sci. 14 (2021) 1.
[46] V. Renuka, B.K. Revathi, D. Reuben Jonathan, M.K. Priya, P. Samuel Asirvatham, Synthesis, growth and characterization of a new NLO active chalcone derivative -4-chloro-N-{3-[(2E)-3-(methoxyphenyl)prop-2-Enoyl]phenyl}benzamide monohydrate, J. Mol. Struct. 1176 (2021) 838–846.
[47] D. Satheesh, R. Roshini, S. Jeevitha, K. Chithra, S. Vasanth Kumar, P. Sellam, Anti-inflammatory and anti-diabetic activity of 8-hydroxyquinolinium 3,5-dinitrobenzoate. 33, 2021, 100726.
[48] C.D. Owen, P. Lukacik, C.M. Strain-Damerell, A. Douangamath, A.J. Powell, D. Fearon, J. Brandao-Neto, A.D. Crawshaw, D. Aragao, M. Williams, R. Flaig, D.R. Hall, K.E. McAuley, M. Mazzorana, D.I. Stuart, F. von Delft, M.A. Walsh SARS-CoV-2 main protease with unliganded active site (2019-nCoV, coronavirus disease 2020, COVID-19). DOI: 10.2210/pdb6YB7/pdb.
[49] M.J. Frisch, G.W. Trucks, H.B. Schlegel, G.E. Scuseria, M.A. Robb, J.R. Cheeseman, G. Scalmani, V. Barone, G.A. Petersson, H. Nakatsuji, X. Li, M. Caricato, A. Marenich, J. Bloino, B.G. Janesko, R. Gomperts, B. Mennucci, H.P. Hratchian, J.V. Ortiz, A.F. Izmaylov, J.L. Sonnenberg, D. Williams-Young, F. Ding, F. Lipparini, F. Egidi, J. Goings, B. Peng, A. Petrone, T. Henderson, D. Ranasinghe, V.G. Zakrzewski, J. Gao, N. Rega, G. Zheng, W. Liang, M. Hada, M. Ehara, K. Toyota, R. Fukuda, J. Hasegawa, M. Ishida, T. Nakajima, Y. Honda, O. Kitao, H. Nakai, T. Vreven, K. Throssell, J.A. Montgomery Jr., J.E. Peralta, F. Ogliaro, M. Bearpark, J.J. Heyd, E. Brothers, K.N. Kudin, V.N. Staroverov, T. Keith, R. Kobayashi, J. Normand, K. Raghavachari, A. Rendell, J.C. Burant, S.S. Iyengar, J. Tomasi, M. Cossi, J.M. Millam, M. Klene, C. Adamo, R. Cammi, J.W. Ochterski, R.L. Martin, K. Morokuma, O. Farkas, J.B. Foresman, D.J. Fox, Gaussian 09, Revision A.02, Gaussian, Inc., Wallingford CT, 2016.
[50] K. Chithra, K. Jayanthi, D. Satheesh, Acetophenone based Mannich bases: synthesis, characterization and their antimicrobial activity, World J. Pharm. Chem. 6 (2) (2017) 1439–1449.
[51] S. Kannan, A. Gomathi, K. Chithra, D. Satheesh, Binuclear copper (II) complexes of salphen-type tetra-imine Schiff's bases derived from 3,3′-diaminobenzidine with 3-allylsalicylaldehyde and 3-ethoxysalicylaldehyde: synthesis, characterization and their antimicrobial activity, Infokara Res. 9 (10) (2020) 236–254.